Available online at www.sciencedirect.com
SCIENCE DIRECT®

Journal of the European Ceramic Society 23 (2003) 2653–2659
www.elsevier.com/locate/jeurceramsoc

Raman spectroscopy of B-site order–disorder in $CaTiO_3$-based microwave ceramics

H. Zheng[a,*], G.D.C. Csete de Györgyfalva[a], R. Quimby[a], H. Bagshaw[a], R. Ubic[b], I.M. Reaney[a], J. Yarwood[c]

[a]*Department of Engineering Materials, University of Sheffield, Sheffield S1 3JD, UK*
[b]*Department of Materials, Queen Mary, University of London, London E1 4NS, UK*
[c]*Materials Research Institute, Sheffield Hallam University, Sheffield S1 1WB, UK*

Abstract

x $CaTiO_3$–$(1-x)$ $Sr(Mg_{1/3}Nb_{2/3})O_3$ (CTSMN) and y $CaTiO_3$–$(1-y)$ $NdAlO_3$ (CTNA) were studied by Raman spectroscopy. A sharp Raman band at 825 cm^{-1} was observed in $SrMg_{1/3}Nb_{2/3}O_3$, consistent with 1:2 long-range ordering of cations on the B-site. The intensity of this band decreased and its width increased with increasing x implying that the degree of order was reduced. A broad Raman band around 800 cm^{-1}, absent in both pure $CaTiO_3$ and $NdAlO_3$, was found in CTNA solid solutions with the strongest intensity at $x=0.5$. The position and intensity of this band suggested that its origin was similar in nature to that observed in CTSMN. The occurrence of a band at $\sim$800 cm^{-1} in CTNA suggested a non-random distribution of Ti^{4+} and Al^{3+} on the B cation sites.

Keywords: Functional applications; Perovskites; Spectroscopy; X-ray methods; $CaTiO_3$; Microwave ceramics

1. Introduction

$CaTiO_3$-based ceramics are attractive candidates for use as dielectric resonators in wireless communication systems. These applications require a combination of high relative permittivity (ε_r), near-zero temperature coefficient of resonant frequency (τ_f) and low dielectric loss (tan δ). $CaTiO_3$ exhibits a high permittivity of 160, accompanied however by a large positive τ_f value ($+850$ ppm/°C).[1] In contrast, other perovskites such as $NdAlO_3$[2] or complex $AB'_xB''_{1-x}O_3$ type perovskites have moderate permittivities of 20–35 combined with small negative τ_f values. Thus, potentially useful ceramics with temperature stable relative permittivities of 40–50 can be obtained by forming solid solutions between $CaTiO_3$ and suitable negative τ_f perovskites.

$AB'_{1/3}B''_{2/3}O_3$ complex perovskites have two different elements B′ and B″ in different oxidation states on the B sites.[3] The microscopic arrangement of such complex compounds is a subject of considerable interest. It is obvious that complex cation arrangements lead to changes in the vibrational spectra in comparison with the starting ABO_3 structure. As a result, Raman scattering can be considered as a probe of the B-site ordering.[3] For example, studies on $PbSc_{1/2}Ta_{1/2}O_3$ (PST) found that the most ordered PST samples displayed narrower and more intense lines in their Raman spectra.[4] $PbMg_{1/3}Nb_{2/3}O_3$ (PMN) with a pseudocubic structure has Mg^{2+} and Nb^{5+} ions on the B-site in a 1:2 ratio. For PMN, local charge compensation in a cubic phase can only be achieved if the B-site ions are distributed randomly, at which point the effective mean symmetry corresponds to the simple perovskite structure, Pm $\bar{3}$m. Nevertheless, Raman spectra from PMN were inconsistent with a cubic structure. No first-order Raman scattering is allowed by symmetry for ideal cubic perovskites, but PMN showed an intense spectrum characteristic of first-order scattering.[5] The initial approach in the interpretation of PMN spectra was to connect the unusual light scattering response by assuming principally that the wave vector selection rules breaks down in PMN due to disorder on the B sublattice. Thus, a contribution

* Corresponding author.

0955-2219/03/$ - see front matter © 2003 Elsevier Ltd. All rights reserved.
doi:10.1016/S0955-2219(03)00149-3

to light scattering should appear from both infrared-active and silent modes.

Although there have been some reports of Raman scattering for simple perovskites such as $CaTiO_3$, $NdAlO_3$ and complex perovksites such as PST and PMN, the Raman spectra of $CaTiO_3$-based solid solutions have not yet been widely studied. The purpose of the present work is therefore, to investigate the vibrational spectra of two series, x $CaTiO_3$–$(1-x)$ $Sr(Mg_{1/3}Nb_{2/3})O_3$ and y $CaTiO_3$–$(1-y)$ $NdAlO_3$ both of which will exhibit a zero τ_f composition at some point in their solid solutions. An attempt was made to clarify the origin of Raman bands and to illustrate the B-site order/disorder effect induced by different substitutions on the B-site.

2. Experimental

Ceramics were synthesised by a conventional mixed oxide route using $CaCO_3$, TiO_2, Nd_2O_3, Al_2O_3, La_2O_3, Ga_2O_3, $SrCO_3$, MgO and Nb_2O_5. The chemical purity of all these raw starting materials was >99%. The weighed starting reagents, in appropriate ratios, were milled (1 μm mean particle size, Laser Coulter Analyser) in propan-2-ol in a high-energy attrition mill (Szegvari Attritor System, Union Process, Ohio, USA) for 2 h, using zirconia media. The slurries were dried and then calcined for 4–6 h at temperatures between 1300 and 1550 °C, depending on composition. Calcined powder was re-milled and then pressed into discs. Discs were sintered for 4 h on zirconia boards at the temperatures between 1500 and 1650 °C. All the fired samples have relative densities above 96%.

An X-ray diffractometer (model PW 1730/10 Philips, Holland) with Cu K_α source ($\lambda = 1.540562$ Å), operated at 50 kV and 30 mA, was used for the identification of phases. A step size of 0.02°, a scan rate of 2°/min, and scan ranges of 10–70° were adopted.

A Renishaw Ramascope System 2000 spectrometer was used for Raman measurements. This system comprised an integral Raman microscope, a stigmatic single spectrograph and a Peltier-cooled CCD detector. The microscope attachment was an Olympus BH2 system and the excitation wavelength used was 633 nm from a He–Ne laser source. Power of 2–3 mW was incident on the samples in a 2 μm diameter spot through a standard ×50 microscope objective lens. The spectra were collected with 30 s data point acquisition time, a spectral range of 150–950 cm^{-1} and a spectral resolution of 3–4 cm^{-1}. Raman spectra were analysed using GRAMS/AI V.7, which is a fully interactive data processing package including peak-fitting, data smoothing, quantitative analysis, peak picking, and integration for Raman spectrum analysis. Spectra were then presented as relative intensity versus Raman shift (cm^{-1} in air).

3. The group-theory prediction of Raman spectra

For simple perovskites $CaTiO_3$ and $NdAlO_3$, factor group analyses have been performed to describe the number and type of modes predicted for each structure.[6] There are a total of 24 Raman-active modes for orthorhombic $CaTiO_3$, Pnma (No. 62) whereas for rhombohedral $NdAlO_3$ $R\bar{3}c$ (No. 167), there are a total of 5 Raman-active modes.

As for the interpretation of vibrational spectra of complex perovskites, two contrary approaches are noted.[4] The first implies that disorder on the B sublattice is responsible for the appearance of first-order Raman scattering features in the spectra, which are connected to the loss of translational and inversion symmetries. In contrast, the second approach implies the existence of ordered regions with a particular symmetry, which allow the appearance of specific Raman modes that are not permitted for cubic materials. These two approaches are not mutually exclusive so a contribution from both is expected in real systems.[4]

In general, the contribution to Raman scattering initiated from the loss of translational symmetry due to disorder on the B sites leads to the broadening of some bands in spectra whereas the narrowing of some bands implies a higher degree of ordering on the B-sites. Siny et al.[3] reported that the order/disorder band in BMT ($BaMg_{1/3}Ta_{2/3}O_3$) was narrower in comparison with those of PMT ($PbMg_{1/3}Ta_{2/3}O_3$), PMN and PST. In these compounds the order/disorder band follows a tendency to reflect the different degree of order; the higher the degree of ordering on the B sites, the smaller the band width. The narrowest width is found in PMW ($PbMg_{1/2}W_{1/2}O_3$), which appears highly ordered compared to PMN and PMT owing to a larger difference in the B-cation charges, Mg^{2+} and W^{6+}.

4. Results and discussion

4.1. X-ray diffraction spectra

Fig. 1 shows XRD spectra of the sintered ceramics of x $CaTiO_3$–$(1-x)$ $Sr(Mg_{1/3}Nb_{2/3})O_3$ series where $x = 0$, 0.2, 0.25, 0.4, 0.5, 0.6, 0.75, 0.9 and 1, respectively. The room-temperature structure of $CaTiO_3$ can be described by Pnma symmetry, resulting from an $a^-a^-c^+$ tilt system[7] and its XRD spectrum may be indexed according to an orthorhombic unit cell (ICDD card: 42-423). The XRD spectrum of $Sr(Mg_{1/3}Nb_{2/3})O_3$ may be indexed according to a hexagonal unit cell ($P\bar{3}m1$), in agreement with ICCD card 17-181. However, work reported by Bagshaw et al.[8] and previously by Steiner et al.[9] clearly demonstrates that SMN undergoes a series of octahedral tilt transitions on cooling, giving rise to an $a^-a^-c^+$ tilt system at room temperature, identical to that of

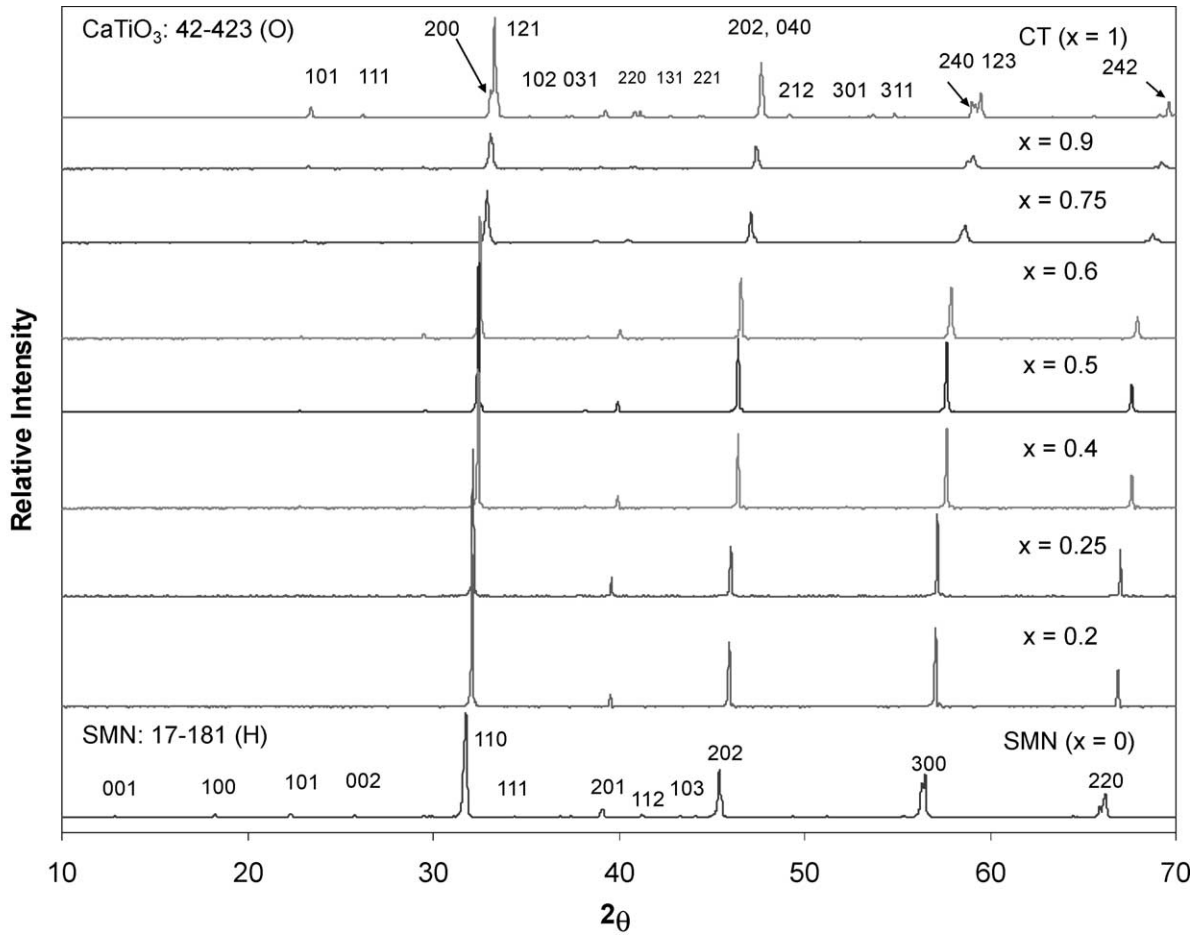

Fig. 1. XRD spectra from x $CaTiO_3$–$(1-x)$ $Sr(Mg_{1/3}Nb_{2/3})O_3$ solid solutions.

$CaTiO_3$. The resulting symmetry is therefore lower than hexagonal, and is probably monoclinic.

There is no evidence of any second phase in the XRD spectra, implying that $Sr(Mg_{1/3}Nb_{2/3})O_3$ and $CaTiO_3$ form a complete solid solution. Equivalent Bragg reflections shift right as x increases, suggesting that lattice parameters decrease with increasing x due to the reduced ionic sizes of both Ca^{2+} (1.35 Å)[10] on the A-site and Ti^{4+} (0.605 Å)[10] on the B-site compared with that of Sr^{2+} (1.44 Å)[10] and $(Mg_{1/3}Nb_{2/3})^{4+}$ (0.67 Å).[10]

Fig. 2 shows XRD spectra from the sintered ceramics of y $CaTiO_3$–$(1-y)$ $NdAlO_3$ series where $y=0$, 0.125, 0.25, 0.375, 0.5, 0.625, 0.75, 0.875 and 1, respectively. The room-temperature structure of $NdAlO_3$ can be described by $R\bar{3}c$ symmetry arising from an $a^-a^-a^-$ tilt system.[7] Its XRD spectrum is indexed using a rhombohedral cell (ICDD card: 71-1596). No second phase is detected throughout this series, suggesting that $NdAlO_3$ and $CaTiO_3$ form a complete solid solution. It is also noticeable that all the corresponding Bragg reflections shift to lower values of 2θ with y, resulting from the lattice expansion as Nd^{3+} (1.09 Å)[10] and Al^{3+} (0.53 Å)[10] are replaced respectively by Ca^{2+} (1.35 Å)[10] and Ti^{4+} (0.605 Å)[10] which have larger ionic radii.

4.2. Raman spectra

Fig. 3 shows the Raman spectra of $CaTiO_3$, $NdAlO_3$ and $Sr(Mg_{1/3}Nb_{2/3})O_3$ in the frequency range 150–950 cm^{-1}, respectively.

The Raman spectrum of $CaTiO_3$ agrees well with that of Hirata et al.,[11] where eight Raman bands are observed at 183, 227, 247, 288, 339, 470, 494 and 641 cm^{-1}. The band observed at 641 cm^{-1} can be assigned to the Ti–O symmetric stretching vibration. Balachandran et al.[12] also attributed a band at $\sim$639 cm^{-1} to Ti–O stretching. The bands at 470 and 494 cm^{-1} are assigned to Ti–O torsional (bending or internal vibration of oxygen cage) modes, in agreement with Hirata et al.[11] and Balachandran et al.[12] The bands in the region 225–340 cm^{-1} are tentatively assigned to the modes associated with rotations of oxygen cage and the band at 183 cm^{-1} is mainly due to the motion of A-site ions.

In the Raman spectrum of $NdAlO_3$, three major scattering bands, centred at 163, 241, 509 cm^{-1}, are observed. The frequencies of these three peaks match well with the previous work.[13] The band at 163 cm^{-1} can be assigned to the mode mainly related to the motion of Nd^{3+} ions. The 509 cm^{-1} band mainly results

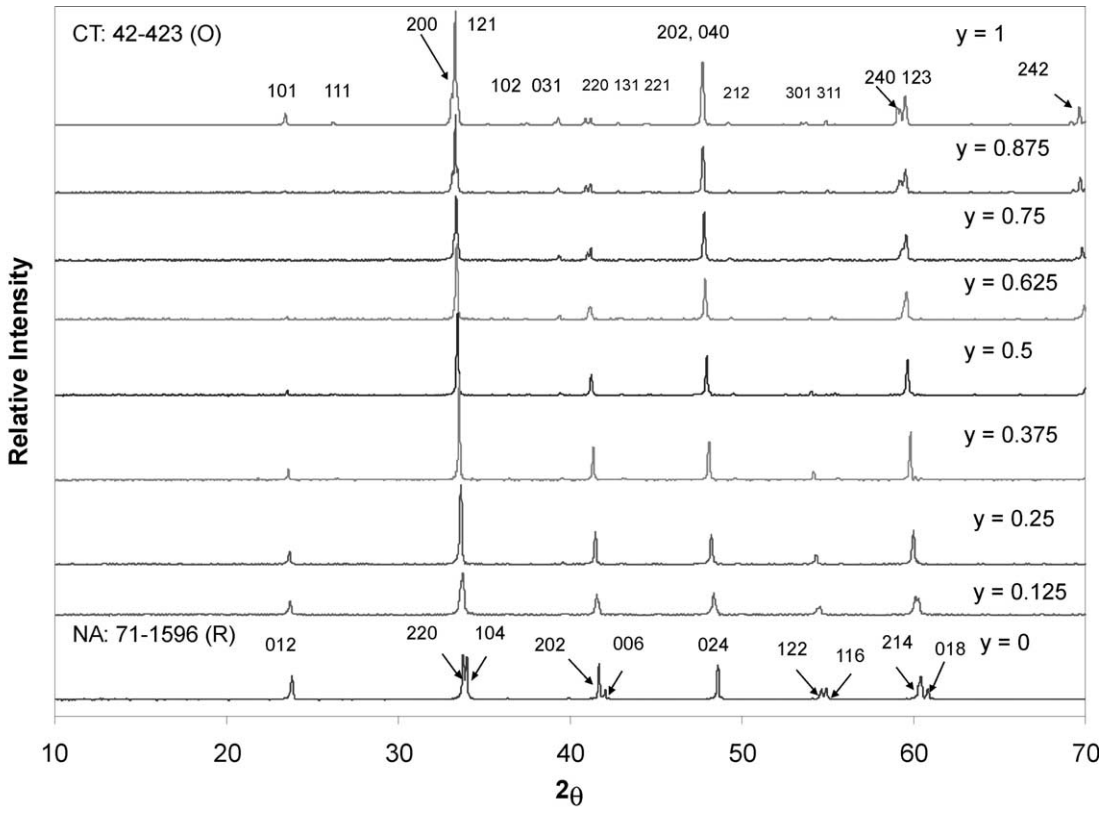

Fig. 2. XRD spectra from y $CaTiO_3$–$(1-y)$ $NdAlO_3$ solid solutions.

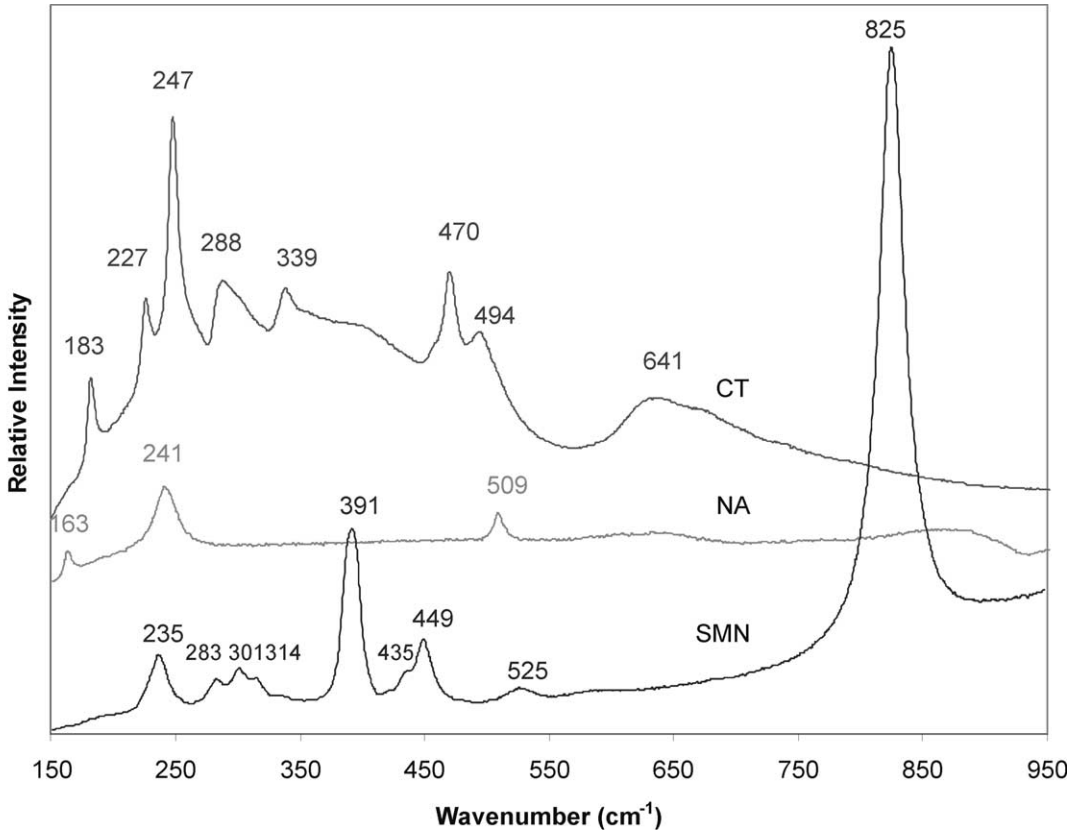

Fig. 3. Raman spectra from $CaTiO_3$, $NdAlO_3$ and $SrMg_{1/3}Nb_{2/3}O_3$.

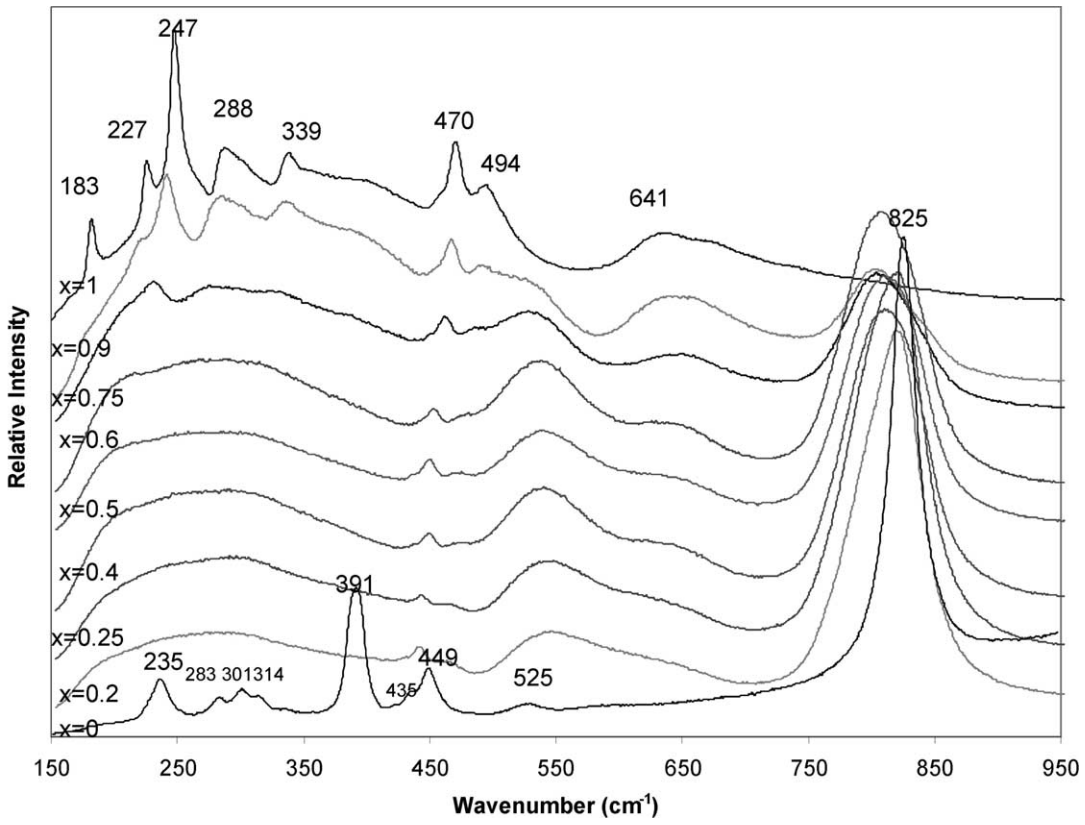

Fig. 4. Raman spectra from x $CaTiO_3$–$(1-x)$ $Sr(Mg_{1/3}Nb_{2/3})O_3$ solid solutions.

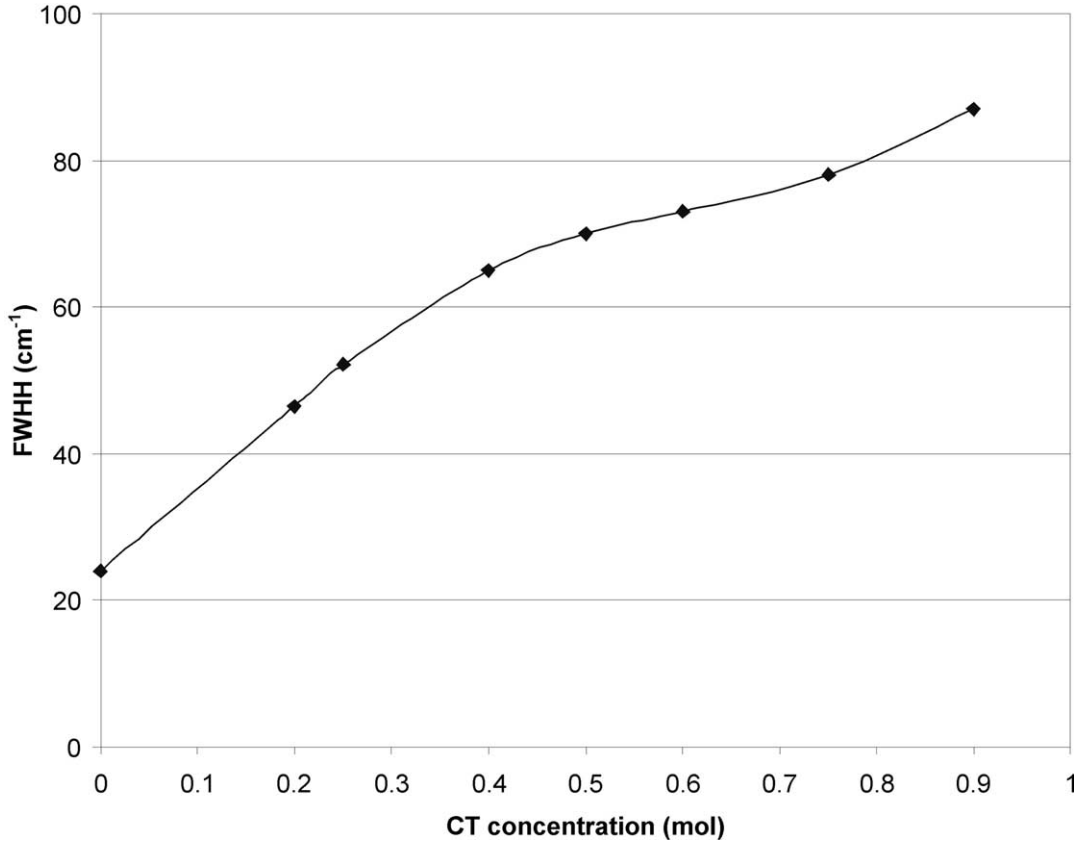

Fig. 5. Full width at half height (FWHH) as a function of CT concentration in CTSMN.

from the internal vibration of the oxygen cage. Harley et al.[14] reported similar bands at 164 cm^{-1} due to the motion of Pr^{3+} ions and 506 cm^{-1} mainly due to the internal oxygen octahedral vibration in $PrAlO_3$. The 241 cm^{-1} band is believed to be associated with out-of-phase rotation of oxygen cage. Granado et al.[15] proposed similar assignments of the Raman frequencies for $NdAlO_3$, in agreement with Sanjuan et al.'s work on $NdGaO_3$.[16]

In the Raman spectrum of $Sr(Mg_{1/3}Nb_{2/3})O_3$ (SMN), nine scattering bands, centred at 235, 283, 301, 314, 391, 435, 449, 525 and 825 cm^{-1}, are observed. Since no relevant work on SMN has been reported, a comparison is not possible here. However, it is most interesting to note the presence of 825 and 391 cm^{-1} bands, which are both absent in $CaTiO_3$ and $NdAlO_3$. The intensities of these two bands are extremely strong and the widths are narrow. It has been suggested that these bands are characteristic of B-site ordering in complex perovskites.[4] Levin et al.[17] observed Raman peaks at 850 and 550 cm^{-1} in ordered $Ca(Al_{0.5}Nb_{0.5})O_3$ and related them to oxygen motions which can be represented as asymmetric and symmetric "breathing" of the $[BO_6]$ octahedra, respectively. The presence of similar bands at 825 and 525 cm^{-1} in SMN suggests that these two bands are primarily associated with the cation ordering on the B sites. The presence of 1:2 B-site ordering is confirmed by transmission electron microscopy (TEM) analysis of Bagshaw et al.[8]

Fig. 4 shows the Raman spectra of $(1-x)$ $Sr(Mg_{1/3}Nb_{2/3})O_3$–x $CaTiO_3$ solid solutions ($x=0-1$). As discussed before, strong and narrow 825 and 391 cm^{-1} bands, absent in $CaTiO_3$, reflect the presence of ordering in SMN. Cation ordering in SMN is driven by the combination of size and charge difference between Mg^{2+} and Nb^{5+}. Thus, Ti^{4+} substitution on the B-site is expected to reduce the driving force for the ordering. As x increases, the bands at 391 and 825 cm^{-1} diminish presumably due to a reduction in the degree of B-site order. The 825 cm^{-1} band also becomes wider with increasing $CaTiO_3$ concentration. Fig. 5 reveals that the full width at half height (FWHH) for the 825 cm^{-1} band increases with x, arising from a reduction in the degree of order. Interestingly, Bagshaw et al.[8] report no ordered $\pm 1/3\{hkl\}$ electron diffraction spots in compounds where $x=0.5$, but the Raman peak is still strong if rather broad.

Fig. 6 shows the Raman spectra of y $CaTiO_3$–$(1-y)$ $NdAlO_3$ series ($y=0-1$). As y increases, several peaks diverge and new Raman-active modes appear. The two bands between 280 and 350 cm^{-1}, labelled as peak **A** and **B**, are not present in pure $NdAlO_3$ and their intensities increase with increasing y. It is thus suggested that

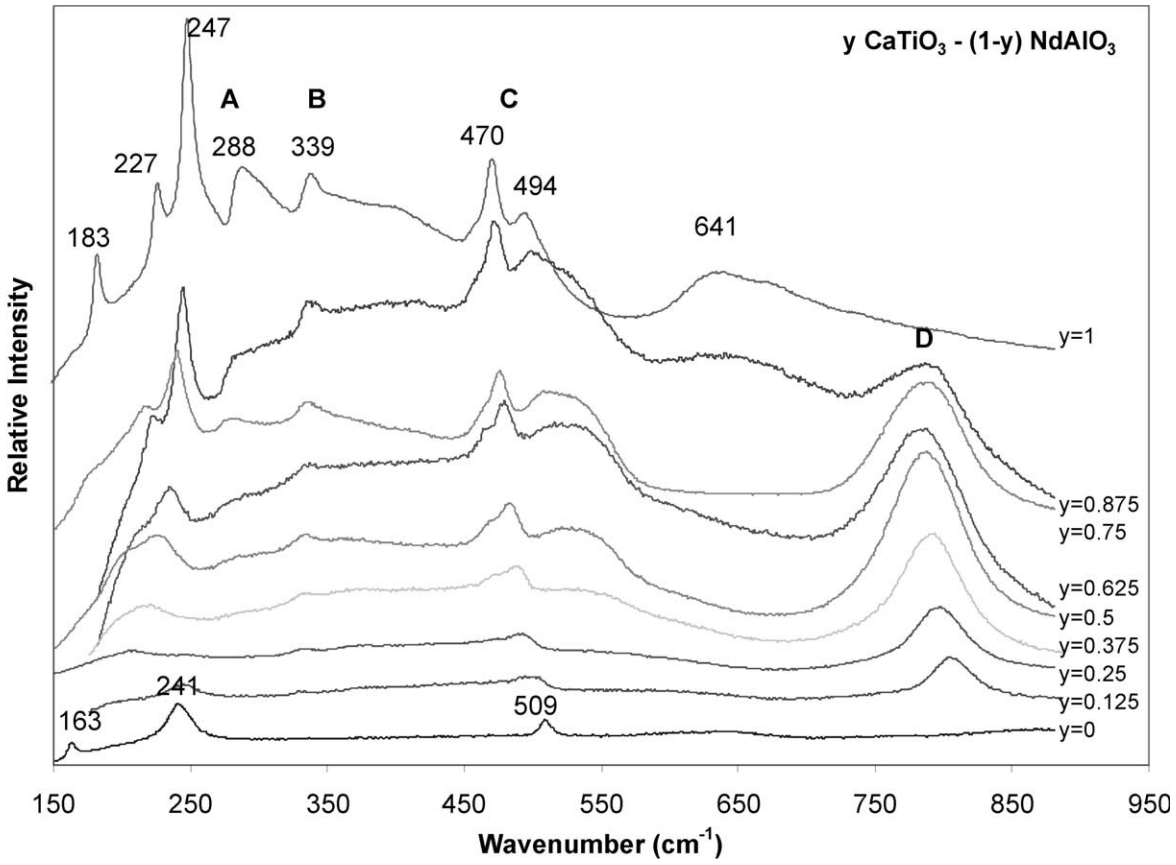

Fig. 6. Raman spectra from y $CaTiO_3$–$(1-y)$ $NdAlO_3$ solid solutions.

these two bands are related to the rotation of oxygen octahedral cage associated with the orthorhombic distortion. The peak around 500 cm^{-1}, labelled **C** (presumably torsional bending bands), is present in the spectra for all the compositions including pure $CaTiO_3$ and $NdAlO_3$. The intensity of this peak increases with increasing y, implying a stronger structural distortion in high-CT compounds.

The broad mode around 800 cm^{-1}, labelled **D**, is absent in both pure $NdAlO_3$ and $CaTiO_3$, but present in all mixed compounds and most intense at $y=0.5$, suggesting that this mode may be related to the cation disorder/order usually observed only in complex perovskites. It is assumed that its nature is similar to the 825 cm^{-1} ordering band observed in SMN except that the peak is much broader, implying the ordering is weak and over a very short range. In CTNA, the B-sites are considered to be occupied randomly by Al^{3+} and Ti^{4+} ions. Due to different ionic sizes and force constants of Al^{3+} and Ti^{4+}, two adjacent corner sharing oxygen octahedra may become nonequivalent. If two octahedra are not equivalent, the constituent oxygen atoms occur in the C_{4v} local positions without an inversion centre and their vibrations become Raman active. This mode is a simple motion of the oxygen atoms like the breathing-type mode of a free oxygen octahedron.[3] As the Ti^{4+} and Al^{3+} are distributed throughout the B sites, there is therefore a distribution of phonon frequencies, resulting in a broad band, characteristic of "disordering" type. More correctly however, it can be interpreted as evidence of a non-random distribution of Al^{3+} and Ti^{4+} on the B-site. No ordered diffraction spots have ever been recorded for CTNA solid solutions but from a simple physical perspective the charge and size difference of Al^{3+} and Ti^{4+} must influence in some way their distribution. These short-range ordering effects can be estimated by considering the integrated intensity of this peak (800 cm^{-1}), which is strongest in CTNA at $x=0.5$.

5. Conclusions

XRD and Raman spectroscopy of x $CaTiO_3$–$(1-x)$ $SrMg_{1/3}Nb_{2/3}O_3$ and y $CaTiO_3$–$(1-y)$ $NdAlO_3$ series were studied. A sharp Raman band at 825 cm^{-1} is observed in $SrMg_{1/3}Nb_{2/3}O_3$, consistent with long-range ordering of cations on the B-site. The intensity of this band falls and its width increases with increasing x implying that the degree of order is reduced. A broad Raman band around 800 cm^{-1}, absent in both pure $CaTiO_3$ and $NdAlO_3$, is found in the CTNA mixed compounds with the strongest intensity at $x=0.5$. The position and intensity of this band suggest that its origin is similar in nature to that observed in CTSMN.

Acknowledgements

Dr. Zheng would like to thank Dr. C.S. Deng at the Materials Research Institute, Sheffield Hallam University for assistance with Raman measurements.

References

1. Wise, P. L., Reaney, I. M., Lee, W. E., Price, T. J., Iddles, D. M. and Cannell, D. S., Structure–microwave property relations in $(Sr_xCa_{(1-x)})_{n+1}Ti_nO_{3n+1}$. *J. Eur. Ceram. Soc.*, 2001, **21**, 1723–1726.
2. Jancar, B., Suvorov, D. and Valant, M., Microwave dielectric properties of $CaTiO_3$–$NdAlO_3$ ceramics. *J. Mat. Sci. Lett.*, 2001, **20**, 71–72.
3. Siny, I. G., Katiyar, R. S. and Bhalla, A. S., Cation arrangement in the complex perovskites and vibrational spectra. *Journal of Raman Spectroscopy*, 1998, **29**, 385–390.
4. Siny, I. G., Tao, R. W., Katiyar, R. S., Guo, R. Y. and Bhalla, A. S., Raman spectroscopy of Mg–Ta order–disorder in $BaMg_{1/3}Ta_{2/3}O_3$. *J. Phys. Chem. Solids*, 1998, **59**(2), 181–195.
5. Burns, G. and Scott, B. A., Index of refraction in "dirty" displacive ferroelectrics. *Solid State Commun.*, 1973, **13**, 423.
6. Tompsett, G. A., Sammes, N. M. and Phillips, R. J., Raman spectroscopy of the $LaGaO_3$ phase transition. *J. Raman Spectroscopy*, 1999, **30**, 497–500.
7. Glazer, A. M., Simple ways of determining perovskite structures. *Acta Crystallogr. A*, 1975, **31**, 756.
8. Bagshaw, H., Reaney, I. M. and Sinclair, D. C. Structure–property relations in $CaTiO_3$ based microwave dielectrics. *J. Eur. Ceram. Soc.* (in press).
9. Steiner, O., Colla, E., Reaney, I. M. and Setter, N., Dielectric behaviour as a function of temperature and structure for the complex perovskites $Ba_xSr_{1-x}(Mg_{1/3},Ta_{2/3})O_3$ and $Ba_xSr_{1-x}(In_{1/2}Nb_{1/2})O_3$. *Conf. Proc. Eur. Ceram. Soc., Madrid*, 1993, **2**, 223–228.
10. Shannon, R. D. and Prewitt, C. T., Effective ionic radii in oxides and fluorides. *Acta Cryst. B*, 1970, **26**, 1046.
11. Hirata, T., Ishioka, K. and Kitajima, M., Vibrational spectroscopy and X-ray diffraction of perovskite compounds $Sr_{1-x}M_xTiO_3$ (M = Ca, Mg; $0 \leqslant x \leqslant 1$). *J. Solid State Chemistry*, 1996, **124**, 353–359.
12. Balachandran, U. and Eror, N. G., Laser-induced Raman scattering in calcium titanate. *Solid State Communications*, 1982, **44**(6), 815–818.
13. Scott, J. F., Raman study of trigonal–cubic phase transitions in rare-earth aluminates. *Physical Review*, 1969, **183**(3), 823–825.
14. Harley, R. T., Hayes, W., Perry, A. M. and Smith, S. R. P., The phase transitions of $PrAlO_3$. *J. Phys. C*, 1973, **6**, 2382–2398.
15. Granado, E., Moreno, N. O., Garcia, A., Sanjurjo, J. A., Rettori, C., Torriani, I., Oseroff, S. B., Neumeier, J. J., McClellan, K. J., Cheong, S. W. and Tokura, Y., Phonon Raman scattering in $R_{1-x}A_xMnO_{3+\delta}$ (R = La, Pr; A = Ca, Sr). *Phys. Rev. B*, 1998, **58**(17), 11435–11440.
16. Sanjuan, M. L., Orera, V. M., Merino, R. I. and Blasco, J., Raman and X-ray study of $La_{1-x}Nd_xGaO_3$ ($0 \leqslant x \leqslant 1$) perovskite solid solutions. *J. Phys.: Condens. Matter*, 1998, **10**, 11687–11702.
17. Levin, I., Chan, J. Y., Geyer, R. G., Maslar, J. E. and Vanerah, T. A., Cation ordering types and dielectric properties in the complex perovskite $Ca(Ca_{1/3}Nb_{2/3})O_3$. *J. Solid State Chem.*, 2001, **156**, 122–134.